A Dual-Band Integrated Network Analyzer for Water Solvent-Specific RF Biosensors

Mayank Awasthi, Syed Azeemuddin, *Senior Member, IEEE*, Annesha Mazumder, and Mohammad Hashmi, *Senior Member, IEEE*

***Abstract*—A solvent-specific novel integrated biosensing network analyzer (IBNA) for the detection of materials with varying dielectric constant (i.e., permittivity) is reported in this article. The proposed IBNA works on the concept that any change in permittivity of the material under test (MUT) results in a change in capacitance of the RF bioliquid cavity's resonant frequency measured by the measurement unit. An interdigitated capacitor-based RF bioliquid cavity resonating at 2.3 GHz performs the sensing operation, while a dual-band six-port reflectometer (DBSPR) with an operating frequency of 1.1 and 2.3 GHz facilitates the measurement of the s-parameters and hence the extraction of permittivities. The DBSPR operating at 1.2 and 2.3 GHz required development of a dual-band coupler which exhibits $|S_{11}|$ of −30 and −25 dB and a bandwidth of 573 and 644 MHz at the chosen design frequencies. It also required design of a dual-band power dividers which possess $|S_{11}|$ of −21.5 and −34.5 dB with a bandwidth of 301 and 264 MHz at the design frequency. The eventual prototype of DBSPR achieves respective bandwidths of 254 and 215 MHz at 1.12 and 2.26 GHz. The resonant frequency of the designed sensing unit loaded with water is 2.483 GHz and this falls in the second band of the DBSPR. Finally, the detection of 1 M Glucose and Sucrose is performed in simulation and experiments and these yield excellent respective frequency shifts of 15 and 20 MHz at room temperature.**

***Index Terms*—Biosensing, dual-band SPR, integrated biosensing network analyzer (IBNA), six-port reflectometer (SPR).**
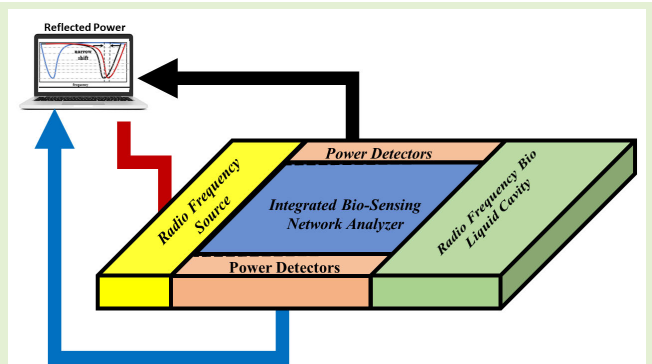
I. INTRODUCTION

THE last two decades has seen an unprecedented interest of the scientific community in radio frequency (RF)-based sensing techniques [1], [2], [3], [4], [5], [6], [7], [8], [9], [10], [11], [12], [13], [14], [15]. It is imperative to note that these techniques offer a number of advantages and can be seamlessly employed in a diverse sets of application domains such as

Mayank Awasthi and Annesha Mazumder are with the CVEST, International Institute of Information Technology Hyderabad, Hyderabad 500032, India.

Syed Azeemuddin is with the CVEST, International Institute of Information Technology Hyderabad, Hyderabad 500032, India, and also with the Department of Electrical and Computer Engineering, University of Mississippi, Oxford, MS 38677 USA.

Mohammad Hashmi is with the School of Engineering and Digital Sciences, Nazarbayev University, Astana 010000, Kazakhstan (e-mail: mohammad.hashmi@nu.edu.kz).

Digital Object Identifier 10.1109/JSEN.2023.3297122

biochemical sensing. The recent literature is replete with reports on bioliquid characterization, biomolecule analysis [1], [2], [3], pathogen detection [4], [5], [7], cell analysis [8], [9], [11], [12], [13], [14], [16], and nanostructure characterization [17], [18]. The key benefits of RF biosensing include cost effectiveness, rapid response, facile, portability and robustness, and a seamless integration with the existing integrated circuits (IC) technology. The detection methodology in such methods essentially studies the variation in the s-parameters of the sensor, such as interdigitated capacitors, coplanar waveguides, and split-ring resonators, in the presence of different materials under test (MUT). The measured s-parameters are then used for the determination and variation in the resonant frequency of the RF bioliquid cavity. Overall, both the broadband and narrowband sensing techniques with extensive qualitative and quantitative analyses have been reported in [19] and [20]. The broadband sensing analyzes the spectrum over a large band of frequencies, whereas the narrowband sensing focuses on the variation in resonance characteristics such as the resonance frequency, amplitude, etc.

A conventional experimental setup for RF-based sensing consists of an RF sensor connected to a vector network
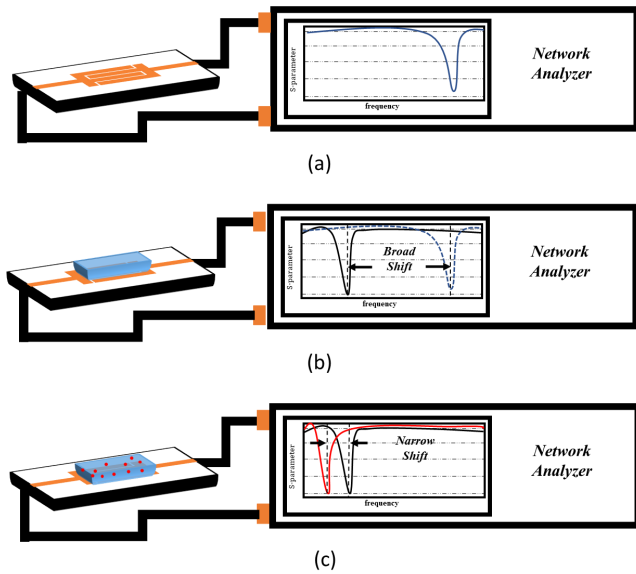
Fig. 1. Shift in frequency at different stages. (a) Empty RF biosensor. (b) Solvent over RF biosensor. (c) Mixture of solvent and solute over RF biosensor.

analyzer (VNA) for measuring the s-parameters. A VNA is a two-port instrument in its simplest form measuring the amplitude and phase information of signals at the ports of RF devices [21], [22], [23], [24], [25], [26]. However, most of these reported sensing setups utilized RF sensor considering air-filled cavities [27], [28], [29]. This complicates the design and analysis procedure considering that in most practical scenarios the samples do not exist in isolation. Instead the samples (i.e., solutes) are first dissolved in solvents such as water, ethanol, and phosphate buffer before test and evaluation. Moreover, these solvents have a higher permittivity when compared to air and this results in very high resonance frequency shifts as can be inferred from (1) and (2). The terms f, L, and C in equations denote the resonant frequency, equivalent inductance, and capacitance, respectively, while ϵ, A, and d have their usual meanings. It is imperative to mention that in general the resonant frequency shifts arising due to the solvent is in the range of GHz and that due to the change in solute is in the range of MHz

$$f = \frac{1}{(2\pi\sqrt{LC})} \tag{1}$$

$$C = \epsilon \cdot \frac{A}{d}. \tag{2}$$

For most practical cases of biosensing, the change in the permittivity is small and hence tiny variations in the resonance frequency need to be measured. However, the traditional broadband VNA-based sensing and measurement setups are typically designed to measure s-parameters of solvents and solutes that result in substantial resonant frequency shifts due to the dramatic changes in their dielectric constant. A pictorial depiction in Fig. 1 is provided for clarity of this aspect. Here, Fig. 1(a)–(c) depicts the respective cases for resonant frequency of an empty RF bioliquid cavity, broad shift in resonance frequency when solvent is placed over RF biosensor,

and a further narrow shift in resonance frequency due to addition of solute in the solvent-loaded biosensor. It has been reported that the detection of minor shifts that occur due to the addition of solutes is often difficult to distinguish from the broad shifts that occur due to solvents. It has been, therefore, agreed in the scientific community that the traditional VNAs are unsuitable for biosensing measurement apart from them being large in size, bulky in nature, and costly. Furthermore, the bandwidth the VNAs deal with is overkill for these applications. This indicates a need for a narrowband solvent-specific platform that can measure the shifts in resonant frequency due to the change in the solutes. In addition, the measurement platform needs to be portable and cost-effective, which are the challenges associated with traditional VNAs.

A number of measurement schemes have been reported in literature to address the limitations of VNA-based measurement setups [30], [31], [32], [33], [34], [35]. For example, the reflectometer reported in [30] operates at a frequency of 2.4 GHz and utilizes AD8302 to measure the reflection coefficient. This setup is seemingly very compact and easy to use but it employs AD8302 which contains mixers and log amplifiers that complicates the design, operation, and maintenance of the reflectometer. The alternative low-cost VNA capable of operating between 4 and 32 GHz appears interesting [31]. However, it consists of multichannel receivers, low noise amplifiers (LNAs), and mixers for the down-conversion of signals. The presence of the complex structure constrains the design process and makes it prone to errors and cost-ineffectiveness. The VNA designed using heterodyne architecture operates between 50 and 100 GHz [32]. Although promising, its operating frequency is beyond the commonly used biosensors and, therefore, its usefulness in biosensing applications is very limited.

To overcome some of the above concerns, a six-port reflectometer (SPR) [33], [34], [35] is utilized in the development of measurement setup. The SPR essentially measures the magnitude and phase of reflected power. However, SPR-based setups in general operate at higher frequencies of 10 GHz and utilize waveguide components and are therefore large and bulky. Therefore, some design aspects need to be resolved to make them practically feasible for biosensing applications. In this context, a tri-band SPR-based platform provides some insights [36]. It utilizes the periodic nature of microstrip lines to produce the other two harmonics of the fundamental frequency. However, this design, although limited in applications to periodic frequencies only, demonstrates a potential for SPR-based biosensors designed for specified frequencies. We also reported a preliminary investigation with some simulation results to demonstrate the feasibility of such a sensing setup based around SPR [37].

From the above discussion, it is clear that an SPR-based setup has potential in biosensing applications [36], [37]. This article, therefore, revisits our SPR-based sensing technique and proposes an integrated biosensing network analyzer (IBNA) exclusively designed for two arbitrary frequencies for the detection of shifts in resonant frequencies. This article essentially builds on the initially reported work in [37] and extends it significantly to develop a fully functional SPR-based
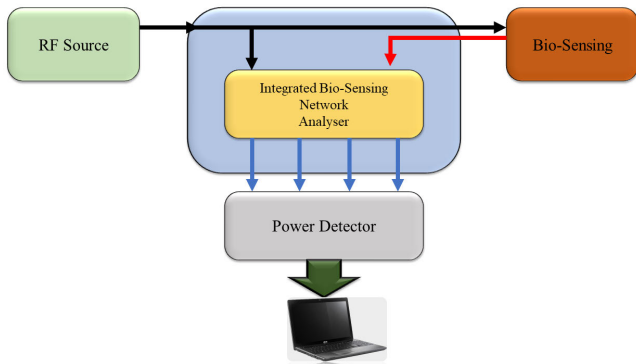
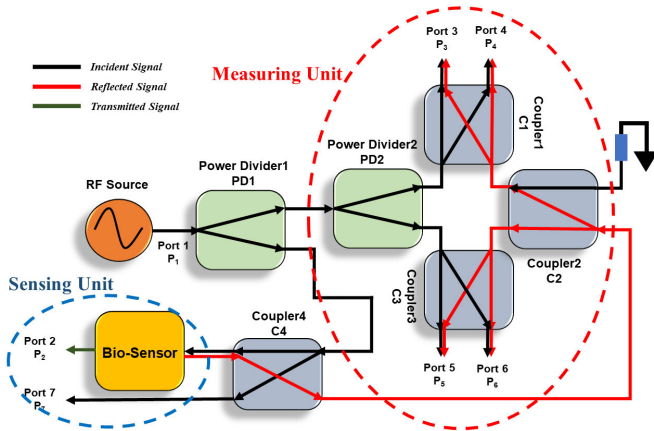Fig. 2. Basic Block diagram of the proposed dual-band integrated network.

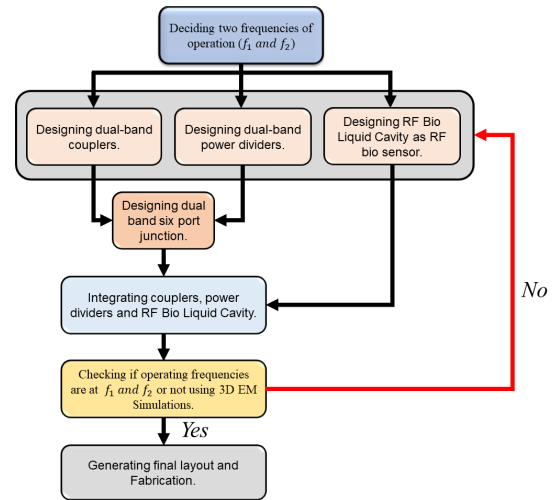Fig. 3. Detailed architecture of the proposed dual-band integrated network analyzer.

Fig. 4. Block diagram of the designing process for IBNA.

a frequency synthesizer, ADF4351 operating in the range of 35–4500 MHz, that acts as an RF source and provides the system's input power to the biosensor. The sensor then reflects a portion of the input power to the four ports (P_3 to P_6) through the internal operation of the couplers and power dividers depicted in Fig. 3. The reflected, incident, and transmitted power are shown in red, black, and green color lines in Fig. 3. Finally, the reflected power is received by power detectors, AD8318 power meters, at ports $P_3 - P_6$ and the collected power is processed, analyzed, and displayed in a computer hosting MATLAB.

The simplified design process of the proposed dual-band IBNA is outlined in Fig. 4. In this work, the commercial RF power source, ADF4351, operates in the range of 35–4500 MHz and hence all other components of the IBNA are designed to work within this frequency range. For example, power dividers and couplers were designed to operate at two distinct bands of 1.1 and 2.3 GHz with narrowband features. Then they are assembled in such a fashion to achieve a fully functional dual-band SPR. For demonstration purpose, an IDC-based water-filled cavity was also designed to work at 2.2 GHz. The cavity and six-port junction are then integrated to develop the proposed IBNA. Final design entails the validation of operating frequencies and other metrics in the simulation software tools such as Keysight ADS and Ansys HFSS. Here, water is utilized as solvent as it has a very stable dielectric constant up to 10 GHz [38]. Glucose and sucrose are then utilized as MUT since their permittivities are close to each other. A brief description of the design procedure of each block is explained in subsequent subsections.

A. Dual-Band Power Divider

One of the key parts of the proposed dual-band IBNA is the dual-band SPR and its realization requires power dividers for the division of power. The two output ports of the power divider PD_1 in Fig. 3 provide power to the sensor and six-port junction. The six-port junction then utilizes that incident power to measure the phase difference between the reflected wave from the sensor and the incident wave. Many reports

measurement and sensing technique for biomedical applications. The proposed IBNA has a unique feature of inbuilt sensing and measurement setups, which no earlier reported designs possess. It presents a complete integrated solution for the detection of materials with different permittivities. The IBNA includes a dual-band SPR (DBSPR) and an RF bioliquid cavity. The dual-band nature here does not depend on transmission lines' periodic behavior. The setup can be used for two different biosamples simultaneously which have constant epsilon in two distinct frequency bands and, therefore, improves the IBNA's reach for practical applications. Furthermore, the impressive power handling capability, small size, affordable cost, and lightweight nature also adds to its superiority over traditional VNA-based sensing setup in measuring the shifts in resonance frequencies. The next sections elaborate on the design techniques of the measurement setup, experimental validation, performance evaluation and benchmarking, and conclusion.

II. PROPOSED DESIGN AND METHODOLOGY

The basic architecture of the proposed dual-band IBNA is given in Fig. 2 and its detailed description is given in Fig. 3. It can be seen that the proposed design integrates a measuring unit (DBSPR) and sensing unit (an RF biosensor). An interdigitated capacitor-based RF bioliquid cavity serves as the biosensor in this case. The proposed system includes
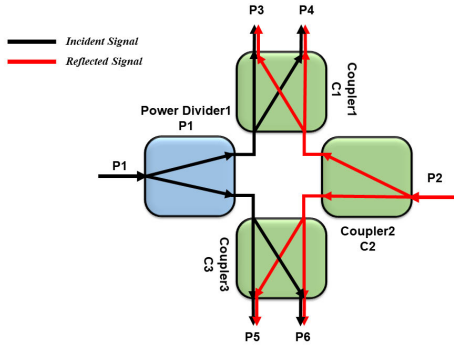
Fig. 5. Block diagram of dual-band six-port network.

employing various approaches have successfully described the procedure for the design of dual-band power divider [39], [40], [41], [42], [43]. For example, the dual-band power dividers design reported in [40] and [43] utilize coupled microstrip lines concept. However, the dual-band power divider reported in [41] presents a very straightforward approach. However, most of these designs result in large power dividers which are not appropriate for biomedical-related applications. Therefore, we adapted the Wilkinson power divider design techniques reported in [44] and [45] to design a dual-band power divider for the chosen frequencies of 1.1 and 2.3 GHz.

B. Dual-Band Coupler Employing Pi-Stub

The couplers are essential in the realization of the eventual IBNA. These are used to separate reflected and incident waves as shown by Coupler4 (C4) in Fig. 3. In the six-port architecture, the three couplers (C1, C2, and C3 in Fig. 3) provide a phase difference of 0°, 90°, 180°, and 270° [46]. Due to these phase differences, constructive and destructive interference occurs, which helps measure the phase difference between reflected and incident waves. Here, the isolation port of Coupler2 (C2) in Fig. 3 is terminated in a 50 Ω to avoid any reflections due to mismatch. In general, the literature is replete with the design strategies of planar stripline coupler. For example, a systematic design technique to design dual-band coupler was reported in [47]. It makes use of Pi-stubs [48], [49] and provides a detailed discussion on the advantages of such an approach. Therefore, the technique reported in [47] is employed to design the dual-band coupler for the proposed IBNA considering that the reported approach is systematic, robust, easily repeatable, and provides excellent performance.

C. Six-Port Network

In the 1970s, the six-port network was introduced by Engen and Hoer [33]. It is a passive structure featuring two input ports and four output ports [50]. It is widely used as a communication receiver [51] for microwave and millimeter wave frequencies. The six-port structure designed using dual-band couplers and power dividers works on the interferometric principle. As shown in Fig. 5, the two input signals P_1 and P_2 get superimposed resulting in constructive and destructive interactions. The power received at the output ports $P_3 - P_6$ then depend upon the magnitude and phase of

the two input signals. Let us assume the two input signals to the six-port network are given by (3) and (4). Here, the terms A, f, and ϕ have usual meanings

$$P_1 = A_1 \cdot e^{j(2\pi f t + \phi_1)} \tag{3}$$

$$P_2 = A_2 \cdot e^{j(2\pi f t + \phi_2)}. \tag{4}$$

The dual-band couplers introduce phase differences at the output ports and generate outputs at respective ports given by (5)–(8) [46]

$$P_3 = K \cdot (P_1 - P_2) \tag{5}$$

$$P_4 = K \cdot j(P_1 + P_2) \tag{6}$$

$$P_5 = K \cdot (P_1 + jP_2) \tag{7}$$

$$P_6 = K \cdot (jP_1 + P_2) \tag{8}$$

where K is the constant due to division of power from couplers and power dividers and, P_3, P_4, P_5, and P_6 are output signals received at four output ports, respectively.

D. Interdigitated Capacitor-Based RF Bioliquid Cavity

Interdigitated capacitors are among the popular classes of RF sensors utilized for biochemical applications [52], [53]. A typical IDC-based sensor consists of several fingers arranged periodically on top of a substrate. The number of fingers and the gap between them directly influence the frequency response of the sensor. Either a common ground is placed below the substrate, or coplanar ground lines are built on the substrate. These sensors are fast, easy to operate and efficient, and are associated with low fabrication complexities and costs. They are characterized by E-Field regions concentrated on top of the fingers and the gap between the fingers. The introduction of samples in these regions generate shifts in the resonance characteristics of the sensors. These shifts, in turn, can be employed to perform both qualitative and quantitative analysis of various MUTs. The design procedure to realize the IDCs are expressed in detail in [54], [55], [56] and [57]. We followed such techniques to design the IDC sensor that meets our frequency specifications. It should be noted that the sensitivity and shifts in the resonant frequency of the designed RF bioliquid cavity depend on the resolution of the frequency generated by the RF source. The RF source with higher resolution is expensive; and therefore, in any setup, the shift in resonant frequency and sensitivity will be related to the resolution of the RF source.

E. Integrated Biosensing Network Analyzer

The components designed in the earlier subsections are integrated, according to Fig. 3, to develop the proposed dual-band IBNA. The input signal was generated by a frequency synthesizer module from Analog Device that consists of ADF4351. The coupler connected to the sensor helps pass the incident signal to the DUT and separate the reflected signal from the incident signal by transferring it to the six-port network's side. Furthermore, the six-port network's output ports (P_3–P_6) are connected with Analog Devices power meter, i.e., AD8318, which measures the output power. The measured output power is then processed using MATLAB
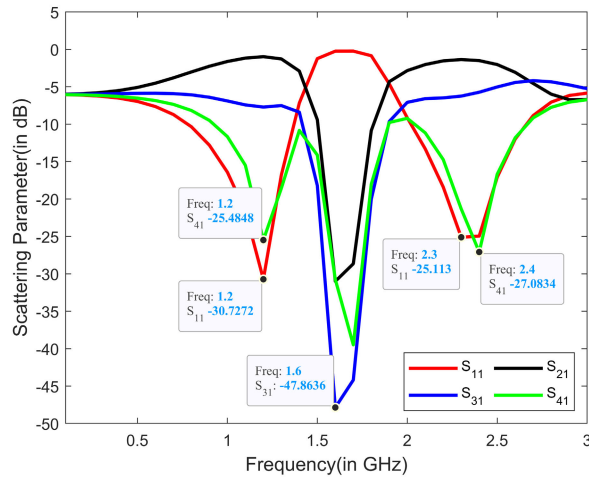
Fig. 6. Performance (in terms of s-parameter) of the dual-band coupler.

hosted in a PC to get the required plots. The magnitudes of the reflection and transmission coefficients is then calculated by (9) and (10). Please refer to Fig. 3 for port numbers

$$|s_{11}| = \frac{|(P_3 - P_4) + j(P_5 - P_6)|}{|P_7|} \quad (9)$$

$$|s_{21}| = |\frac{P_2}{P_7}| \quad (10)$$

where $P_3 - P_7$ are the power at the respective ports marked in Fig. 3. It should be noted that although the above equations can be utilized to measure phase as well, the focus of this work is only on magnitude measurement.

It is pertinent to mention that the developed IBNA is scalable for other frequencies and solvents. For other solvents, there is a need to consider the range of frequencies for which the selected solvent has constant permittivity. Thereafter, the SPR components and RF biosensor need to be redesigned to work in that specific frequency range.

III. SIMULATION RESULTS

The proposed six-port network's components and IDC-based RF biosensor were designed using RT Duroid 5880 as the substrate material whose parameters are listed below. Subsequently, simulation was carried out using AWR Microwave office and CST 3-D EM simulator. Just to keep the things in perspectives, the operating frequencies for the proposed design are 1.1 and 2.3 GHz.

1) Height, $h_s = 1.6$ mm.
2) Dielectric constant, $\epsilon_r = 2.2$.
3) Tangent loss, $\tan \delta = 0.0037$.
4) Top copper layer thickness, $T_{top} = 35$ μm.
5) Bottom copper layer thickness, $T_{bottom} = 35$ μm.

A. Dual-Band Coupler

The performance, in terms of s-parameters, of the designed coupler is depicted in Fig. 6. As mentioned earlier, this work made use of pi-stub in the design of dual-band coupler [47]. It can be observed that the coupler operates at 1.2 and 2.3 GHz having excellent matching at port-1 which can be
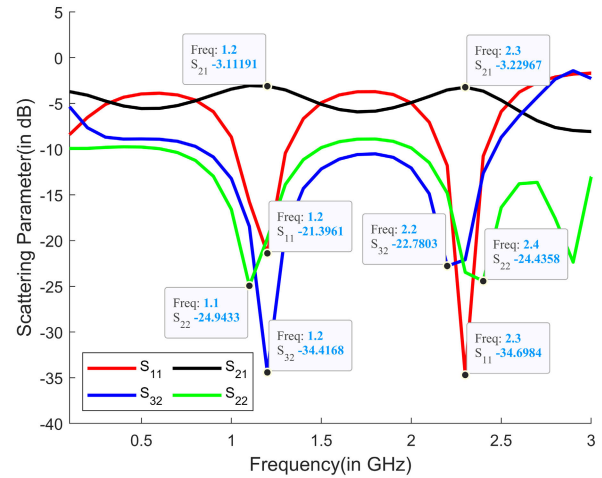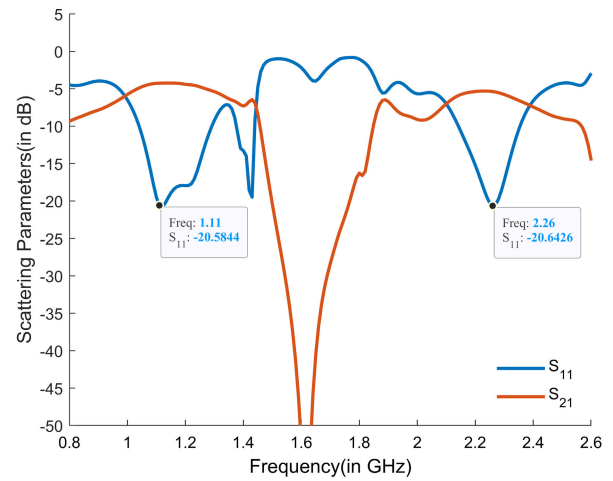

Fig. 7. S-parameter for dual-band power divider.

Fig. 8. S-parameter for DBSPR demonstrating excellent performance.

inferred from $|s_{11}|$ (reflection coefficient) of -30 and -25 dB. Furthermore, the -10 dB bandwidth at the operating frequencies are 573 and 644 MHz, respectively

B. Dual-Band Power Divider

As the proposed design requires power dividers, a dual-band power divider was designed and simulated. Fig. 7 shows the simulation results. It shows $|s_{11}|$ of -21.5 and -34.5 dB with bandwidth of 301 and 264 MHz, respectively, at the chosen frequencies of 1.2 and 2.3 GHz. It also exhibits high isolation of -34.4 and -23 dB, respectively.

C. Dual-Band Six-Port Reflectometer

The DBSPR as per Fig. 5 was designed by integrating the already designed dual-band couplers and power dividers and simulated for the operating frequencies of 1.1 and 2.3 GHz. It can be inferred from Fig. 8 that the designed DBSPR possesses -10 dB bandwidth of 254 and 215 MHz at the operating frequencies of 1.12 and 2.26 GHz, respectively. Moreover, the DBSPR achieves a very high transmission zero of less than -50 dB, which makes it work in its two operating bands.
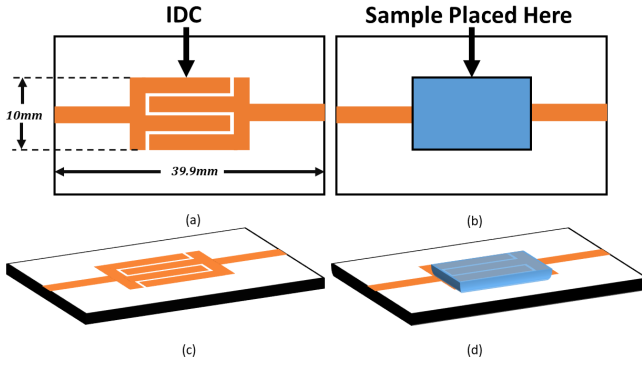
Fig. 9. IDC-based RF biosensor. (a) Top view. (b) Top view with sample. (c) Bird's eye view. (d) Bird's eye view with sample.
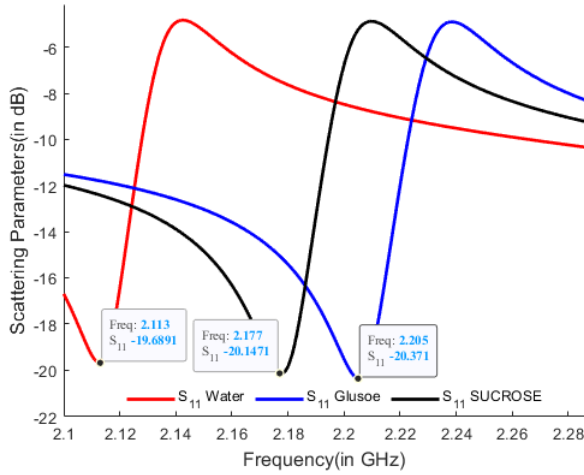

Fig. 11. S_{11} achieved using simulation for IBNA with different MUTs having 1 Molar concentration with different permittivities.
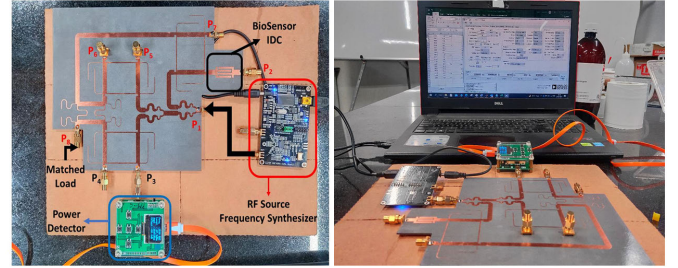
Fig. 12. Fabricated IBNA with power detectors and frequency synthesizers.

Fig. 10. S_{11} for interdigitated capacitor RF bio sensor.
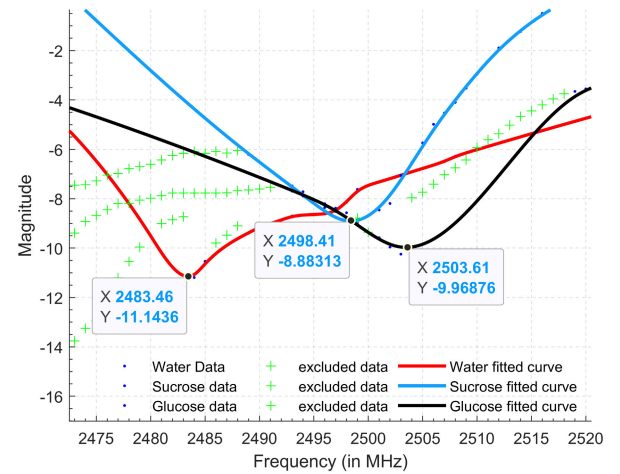
Fig. 13. Experimental results using glucose, sucrose, and water.

D. Interdigitated Capacitor-Based RF Bioliquid Cavity

For the demonstration of the developed sensing system, a single band RF bioliquid cavity was designed and simulated. Fig. 9 shows the structure of RF bioliquid cavity and the placement of the sample over it. Moreover, Fig. 10 presents the reflection coefficient and shift in resonant frequency when the sensor was loaded with water, glucose, and sucrose. Shifts of 64 and 92 MHz was observed when material was changed from water to sucrose and glucose, respectively.

E. IBNA With Glucose and Sucrose (MUT)

As described previously, the simulation mimicked the practical way of changing materials with different permittivities over the designed RF bioliquid cavity. The results in Fig. 11 show that the permittivity changes every time the material changes, and hence, a shift in resonant frequency is observed. Here, in this case, when the material was water, the resonant frequency was at 2.23 GHz and as the material is changed to sucrose and glucose, the resonant frequency shifts toward right as identified by the proposed IBNA. In essence, the simulation results demonstrate the ability of the proposed IBNA in sensing the shifts in resonant frequencies with changing solutes.

IV. EXPERIMENTAL SETUP AND MEASUREMENTS

Fig. 12 shows the experimental setup for IBNA. The frequency synthesizer (ADF4351) is used as an RF source, and it generates frequencies from 30 to 4500 MHz [64]. Also, AD8318 [65] was used as a power detector for measuring power received at the respective output ports. Furthermore, the data of the power measured at the four ports were transferred to PC possessing MATLAB and final plots were generated as shown in Fig. 13. It should be noted that the volume of

TABLE I
COMPARISON OF MULTIPORT REFLECTOMETER PERFORMANCE

Parameters	[58]	[59]	[60]	[61]	[62]	[51]	[63]	This Work
Application	general purpose	general purpose	permittivity sensor	CW Radar	communication receiver	CW Radar	general purpose	permittivity sensor
Freq. range (GHz)	2.5-3.5	55-65	1.9-2.058, 15.2-16.6	24	2.45	75-84	1-10	1.05-1.3, 2.14 - 2.35
Bandwidth ratio (f_1/f_2)	1.4	1.18	1.09	1	1	1.12	10	1.23, 1.19
Technology	PCB Stripline	MHMIC	MEMS	PCB Microstripline	PCB Microstripline	SiGe MMIC	PCB Microstripline	PCB Microstripline
Size (mm× mm)	56× 49	15×15	6.8×50 with VCO, Power Detector, Sensor	-	-	1.03×1.13 with Power Detector, LNA	-	150×200
Topology	multi detector	multi detector	multi-state reflectometer	multi detector	multi detector	multi detector	multi detector	multi detector
No. of Power Detector	4	4	1	4	2	4	2	4
Design complexity	medium	medium	high	medium	medium	high	medium	low

TABLE II
PRICE COMPARISON OF CURRENTLY AVAILABLE VNAS

Price Comparison	
Setup	Cost(in USD)
N9914B FieldFox Handheld RF Analyzer, 6.5 GHz	20,418
NanoVNA V2 Plus4 from HCXQS group, 4GHz	280
Proposed Design	235

the samples and temperature of the room was kept constant at 400 μl and 25 °C. For performing the experiment, the following materials with different permittivities were chosen.

1) Distilled water ($\epsilon_w = 79$).
2) Sucrose ($\epsilon_s = 74$).
3) Glucose ($\epsilon_g = 72$)

where ϵ_w, ϵ_s, and ϵ_g represent the permittivity of the respective materials. It is imperative to note that the frequency of operation in this case was 2.4 GHz with a bandwidth of around 200 MHz as mentioned earlier. Therefore, only this specific frequency range has been investigated in this case study and the rest of the data have been excluded. For testing purposes, 1 M solutions of glucose and sucrose in water were used. Subsequently, 400 μl of the liquids was gently dropped over the sensitive area of the IDC. It can be observed from Fig. 13 that a resonant frequency of 2483 MHz was achieved when the RF bioliquid cavity was loaded with water. However, shifts of 15 and 20 MHz were observed when the material was changed from water to sucrose and glucose, respectively. This clearly demonstrates that the proposed sensor setup can measure the shift in frequencies owing to the change in permittivities of solvents.

To present the advantages of the proposed IBNA, it has been compared with other reported designs in Table I. It can be clearly inferred from Table I that the proposed IBNA exhibits superiority in most of the aspects over the other sensors reported in the literature. Table II presents a price comparison with currently available VNAs in the industry which proves the cost-effectiveness of IBNA. Moreover, the proposed IBNA also has a unique feature of inbuilt sensing and measurement setups, which no earlier reported designs possess. Furthermore, for better reliability, the setup can be covered in a metallic shield to safeguard against any external noise and interference.

V. CONCLUSION

A Dual-Band SPR-based RF biosensor is conceptualized, analyzed, designed, and experimentally validated for its ability to measure the magnitude of the reflected signal. A generalized approach for the design of an IBNA is developed by integrating power dividers, couplers, and RF bioliquid cavity with DBSPR. The proposed setup successfully detects and measures the shift in resonant frequencies when materials with different permittivities are used as MUT. A resonant frequency of 2483 MHz was achieved when the RF bioliquid cavity was loaded with water, and shifts of 15 and 20 MHz in the resonant frequency were observed when the material was changed from water to sucrose and glucose, respectively. The results are promising and, therefore, have the potential as a cost-effective and efficient alternative for biochemical applications. However, some challenges, such as high form factor at low frequencies and broader bandwidth, are some minor issues which need redressal in future. Furthermore, the proposed IBNA's precision relies on the quality of the RF source and noise figure in the power detectors. Therefore, appropriate care should be taken to choose and test these off-the-shelf components before their use in the IBNA setup.

REFERENCES

[1] J. C. Booth, N. D. Orloff, J. Mateu, M. Janezic, M. Rinehart, and J. A. Beall, "Quantitative permittivity measurements of nanoliter liquid volumes in microfluidic channels to 40 GHz," *IEEE Trans. Instrum. Meas.*, vol. 59, no. 12, pp. 3279–3288, Dec. 2010.

[2] J. Mateu, N. Orloff, M. Rinehart, and J. C. Booth, "Broadband permittivity of liquids extracted from transmission line measurements of microfluidic channels," in *IEEE MTT-S Int. Microw. Symp. Dig.*, Jun. 2007, pp. 523–526.

[3] I. Ocket et al., "Dielectric characterization of biological liquids and tissues up to 110 GHz using an LTCC CPW sensor," in *Proc. IEEE Topical Conf. Biomed. Wireless Technol., Netw., Sens. Syst.*, Jan. 2013, pp. 43–45.

[4] D. Elsheakh, H. Elsadek, E. Abdullah, S. Atteya, and W. N. Elmazny, "Novel rapid detection of different viruses in blood using microimmunosensor," in *Proc. 7th Eur. Conf. Antennas Propag. (EuCAP)*, Apr. 2013, pp. 1128–1131.

[5] R. Narang et al., "Sensitive, real-time and non-intrusive detection of concentration and growth of pathogenic bacteria using microfluidic-microwave ring resonator biosensor," *Sci. Rep.*, vol. 8, no. 1, pp. 1–10, Oct. 2018.

[6] D. Rano and M. Hashmi, "Extremely compact EBG-backed antenna for smartwatch applications in medical body area network," *IET Microw., Antennas Propag.*, vol. 13, no. 7, pp. 1031–1040, Jun. 2019.

[7] H.-J. Lee et al., "A planar split-ring resonator-based microwave biosensor for label-free detection of biomolecules," *Sens. Actuators B, Chem.*, vol. 169, pp. 26–31, Jul. 2012.

[8] M. Nikolic-Jaric et al., "Microwave frequency sensor for detection of biological cells in microfluidic channels," *Biomicrofluidics*, vol. 3, no. 3, Sep. 2009, Art. no. 034103.

[9] K. Grenier et al., "Resonant based microwave biosensor for biological cells discrimination," in *Proc. IEEE Radio Wireless Symp. (RWS)*, Jan. 2010, pp. 523–526.

[10] D. Rano and M. Hashmi, "Interdigital based EBG: Compact and polarization stable for MBAN and Wi-Fi," in *Proc. 12th Eur. Conf. Antennas Propag. (EuCAP)*, Apr. 2018, pp. 1–5.

[11] A. Peyman et al., "Variation in dielectric properties due to pathological changes in human liver," *Bioelectromagnetics*, vol. 36, no. 8, pp. 603–612, Dec. 2015.

[12] H.-W. Wu, "Label-free and antibody-free wideband microwave biosensor for identifying the cancer cells," *IEEE Trans. Microw. Theory Techn.*, vol. 64, no. 3, pp. 982–990, Mar. 2016.

[13] C. Dalmay, J. Leroy, A. Pothier, and P. Blondy, "Development of high frequency microfluidic biosensors for intracellular analysis," *Proc. Eng.*, vol. 87, pp. 54–57, Jan. 2014.

[14] N. M. Haase, G. Fuge, H. K. Trieu, A.-P. Zeng, and A. F. Jacob, "Miniaturized transmission-line sensor for broadband dielectric characterization of biological liquids and cell suspensions," *IEEE Trans. Microw. Theory Techn.*, vol. 63, no. 10, pp. 3026–3033, Oct. 2015.

[15] D. Rano and M. Hashmi, "Design and analysis of wearable patch antenna array for MBAN applications," in *Proc. 22nd Nat. Conf. Commun. (NCC)*, Mar. 2016, pp. 1–6.

[16] L. Yan Zhang et al., "Microwave biosensors for identifying cancer cell aggressiveness grade," in *IEEE MTT-S Int. Microw. Symp. Dig.*, Jun. 2012, pp. 1–3.

[17] A. Mazumder, S. Azeemuddin, T. K. Sau, and P. Bhimalapuram, "Study of gold particles in HFSS with varying physical parameters and arrangements," in *Proc. IEEE 15th Int. Conf. Nano/Micro Engineered Mol. Syst. (NEMS)*, Sep. 2020, pp. 529–532.

[18] A. Mazumder, S. Azeemuddin, T. K. Sau, and P. Bhimalapuram, "Role of shape of gold nanoparticles in sensing biomolecules using radio-frequency based sensors," in *Proc. IEEE Sensors*, Oct. 2020, pp. 1–4.

[19] K. Wadhwani, S. Hussaini, and A. Syed, "Real-time qualitative and quantitative analysis of saccharides using CSRR based RF sensor," in *Proc. IEEE Sensors*, Oct. 2022, pp. 1–4.

[20] K. Wadhwani, S. Hussaini, A. Mazumder, and A. Syed, "Solvent-based optimization of CSRR and IDC RF bio-sensors," *IEEE Sensors J.*, vol. 22, no. 6, pp. 5651–5661, Mar. 2022.

[21] M. Alibakhshi-Kenari, M. Naser-Moghadasi, R. A. Sadeghzadeh, and B. S. Virdee, "Hexa-band planar antenna with asymmetric fork-shaped radiators for multiband and broadband communication applications," *IET Microw., Antennas Propag.*, vol. 10, no. 5, pp. 471–478, Apr. 2016.

[22] M. Alibakhshi-Kenari, M. Naser-Moghadasi, R. A. Sadeghzadeh, B. S. Virdee, and E. Limiti, "New CRLH-based planar slotted antennas with helical inductors for wireless communication systems, RF-circuits and microwave devices at UHF–SHF bands," *Wireless Pers. Commun.*, vol. 92, no. 3, pp. 1029–1038, Feb. 2017.

[23] M. Alibakhshi-Kenari, M. Naser-Moghadasi, R. A. Sadeghzadeh, B. S. Virdee, and E. Limiti, "Miniature CRLH-based ultra wideband antenna with gain enhancement for wireless communication applications," *ICT Exp.*, vol. 2, no. 2, pp. 75–79, Jun. 2016.

[24] M. Alibakhshikenari et al., "Dual-polarized highly folded Bowtie antenna with slotted self-grounded structure for sub-6 GHz 5G applications," *IEEE Trans. Antennas Propag.*, vol. 70, no. 4, pp. 3028–3033, Apr. 2022.

[25] M. Alibakhshikenari et al., "Impedance bandwidth improvement of a planar antenna based on metamaterial-inspired T-matching network," *IEEE Access*, vol. 9, pp. 67916–67927, 2021.

[26] A. Raza, A. Jabbar, D. A. Sehrai, H. Atiq, and R. Ramzan, "SDR based VNA for characterization of RF sensors and circuits," in *Proc. 1st Int. Conf. Microw., Antennas Circuits (ICMAC)*, Dec. 2021, pp. 1–4.

[27] J. Yeo and J.-I. Lee, "High-sensitivity microwave sensor based on an interdigital-capacitor-shaped defected ground structure for permittivity characterization," *Sensors*, vol. 19, no. 3, p. 498, Jan. 2019.

[28] A. A. M. Bahar, Z. Zakaria, M. K. M. Arshad, A. A. M. Isa, Y. Dasril, and R. A. Alahnomi, "Real time microwave biochemical sensor based on circular SIW approach for aqueous dielectric detection," *Sci. Rep.*, vol. 9, no. 1, pp. 1–12, Apr. 2019.

[29] M. A. H. Ansari, A. K. Jha, and M. J. Akhtar, "Design and application of the CSRR-based planar sensor for noninvasive measurement of complex permittivity," *IEEE Sensors J.*, vol. 15, no. 12, pp. 7181–7189, Dec. 2015.

[30] D. K. Huynh and G. Zimmer, "Reflectometer with complete error correction," in *Proc. Int. Conf. Adv. Technol. Commun. (ATC)*, Oct. 2018, pp. 133–141.

[31] J. Nehring et al., "Highly integrated 4–32-GHz two-port vector network analyzers for instrumentation and biomedical applications," *IEEE Trans. Microw. Theory Techn.*, vol. 65, no. 1, pp. 229–244, Jan. 2017.

[32] I. Nasr, J. Nehring, K. Aufinger, G. Fischer, R. Weigel, and D. Kissinger, "Single- and dual-port 50–100-GHz integrated vector network analyzers with on-chip dielectric sensors," *IEEE Trans. Microw. Theory Techn.*, vol. 62, no. 9, pp. 2168–2179, Sep. 2014.

[33] G. F. Engen and C. A. Hoer, "Application of an arbitrary 6-port junction to power-measurement problems," *IEEE Trans. Instrum. Meas.*, vol. IM-21, no. 4, pp. 470–474, Nov. 1972.

[34] C. A. Hoer, "The six-port coupler: A new approach to measuring voltage, current, power, impedance, and phase," *IEEE Trans. Instrum. Meas.*, vol. IM-21, no. 4, pp. 466–470, Nov. 1972.

[35] G. F. Engen, "The six-port reflectometer: An alternative network analyzer," *IEEE Trans. Microw. Theory Techn.*, vol. MTT-25, no. 12, pp. 1075–1080, Dec. 1977.

[36] S. Linz, M. Hofmann, G. Fischer, R. Weigel, and D. Kissinger, "A multiband 2-port vector network analyzer based on six-port junctions for biomedical measurement applications between 6 GHz and 33 GHz," in *Proc. IEEE-APS Topical Conf. Antennas Propag. Wireless Commun. (APWC)*, Sep. 2013, pp. 532–535.

[37] M. Awasthi, K. Wadhwani, A. Syed, and M. Hashmi, "A dual-band integrated network analyzer for RF bio sensing application," in *Proc. IEEE Asia–Pacific Microw. Conf. (APMC)*, Dec. 2020, pp. 196–198.

[38] A. Andryieuski, S. M. Kuznetsova, S. V. Zhukovsky, Y. S. Kivshar, and A. V. Lavrinenko, "Water: Promising opportunities for tunable all-dielectric electromagnetic metamaterials," *Sci. Rep.*, vol. 5, no. 1, pp. 1–9, Aug. 2015.

[39] M. A. Maktoomi and M. S. Hashmi, "A performance enhanced port extended dual-band Wilkinson power divider," *IEEE Access*, vol. 5, pp. 11832–11840, 2017.

[40] Y. Wu, Y. Liu, and Q. Xue, "An analytical approach for a novel coupled-line dual-band Wilkinson power divider," *IEEE Trans. Microw. Theory Techn.*, vol. 59, no. 2, pp. 286–294, Feb. 2011.

[41] F.-X. Liu and J.-C. Lee, "Design of new dual-band Wilkinson power dividers with simple structure and wide isolation," *IEEE Trans. Microw. Theory Techn.*, vol. 67, no. 9, pp. 3628–3635, Sep. 2019.

[42] M. A. Maktoomi, M. S. Hashmi, and F. M. Ghannouchi, "Theory and design of a novel wideband DC isolated Wilkinson power divider," *IEEE Microw. Wireless Compon. Lett.*, vol. 26, no. 8, pp. 586–588, Aug. 2016.

[43] M. H. Maktoomi, D. Banerjee, and M. S. Hashmi, "An enhanced frequency-ratio coupled-line dual-frequency Wilkinson power divider," *IEEE Trans. Circuits Syst. II, Exp. Briefs*, vol. 65, no. 7, pp. 888–892, Jul. 2018.

[44] H. Oraizi and A.-R. Sharifi, "Design and optimization of broadband asymmetrical multisection Wilkinson power divider," *IEEE Trans. Microw. Theory Techn.*, vol. 54, no. 5, pp. 2220–2231, May 2006.

[45] M. M. Honari, L. Mirzavand, R. Mirzavand, A. Abdipour, and P. Mousavi, "Theoretical design of broadband multisection Wilkinson power dividers with arbitrary power split ratio," *IEEE Trans. Compon., Packag., Manuf. Technol.*, vol. 6, no. 4, pp. 605–612, Apr. 2016.

[46] A. Koelpin, G. Vinci, B. Laemmle, D. Kissinger, and R. Weigel, "The six-port in modern society," *IEEE Microw. Mag.*, vol. 11, no. 7, pp. 35–43, Dec. 2010.

[47] M. A. Maktoomi, M. S. Hashmi, and F. M. Ghannouchi, "Systematic design technique for dual-band branch-line coupler using T- and Pi-networks and their application in novel wideband-ratio crossover," *IEEE Trans. Compon., Packag., Manuf. Technol.*, vol. 6, no. 5, pp. 784–795, May 2016.

[48] M. A. Maktoomi and M. S. Hashmi, "A coupled-line based L-section DC-isolated dual-band real to real impedance transformer and its application to a dual-band T-junction power divider," *Prog. Electromagn. Res. C*, vol. 55, pp. 95–104, 2014.

[49] M. A. Maktoomi, M. S. Hashmi, and F. M. Ghannouchi, "Improving load range of dual-band impedance matching networks using load-healing concept," *IEEE Trans. Circuits Syst. II, Exp. Briefs*, vol. 64, no. 2, pp. 126–130, Feb. 2017.

[50] F. M. Ghannouchi and A. Mohammadi, *The Six-Port Technique With Microwave and Wireless Applications*. Norwood, MA, USA: Artech House, 2009.

[51] B. Laemmle, G. Vinci, L. Maurer, R. Weigel, and A. Koelpin, "A 77-GHz SiGe integrated six-port receiver front-end for angle-of-arrival detection," *IEEE J. Solid-State Circuits*, vol. 47, no. 9, pp. 1966–1973, Sep. 2012.

[52] J. W. Kim, "Development of interdigitated capacitor sensors for direct and wireless measurements of the dielectric properties of liquids," Elect. Comput. Eng., Univ. Texas Austin, Austin, TX, USA, Tech. Rep., 2008.

[53] E. Hammerstad and O. Jensen, "Accurate models for microstrip computer-aided design," in *IEEE MTT-S Int. Microw. Symp. Dig.*, Mar. 1980, pp. 407–409.

[54] M. K. Krage and G. I. Haddad, "Frequency-dependent characteristics of microstrip transmission lines," *IEEE Trans. Microw. Theory Techn.*, vol. MTT-20, no. 10, pp. 678–688, Oct. 1972.

[55] S. S. Gevorgian, T. Martinsson, P. L. J. Linner, and E. L. Kollberg, "CAD models for multilayered substrate interdigital capacitors," *IEEE Trans. Microw. Theory Techn.*, vol. 44, no. 6, pp. 896–904, Jun. 1996.

[56] P. H. Aaen, J. A. Pla, and C. A. Balanis, "On the development of CAD techniques suitable for the design of high-power RF transistors," *IEEE Trans. Microw. Theory Techn.*, vol. 53, no. 10, pp. 3067–3074, Oct. 2005.

[57] A. V. Mamishev, K. Sundara-Rajan, F. Yang, Y. Du, and M. Zahn, "Interdigital sensors and transducers," *Proc. IEEE*, vol. 92, no. 5, pp. 808–845, May 2004.

[58] K. Staszek, S. Gruszczynski, and K. Wincza, "Six-port reflectometer providing enhanced power distribution," *IEEE Trans. Microw. Theory Techn.*, vol. 64, no. 3, pp. 939–951, Mar. 2016.

[59] K. Haddadi and T. Lasri, "Forward V-band vector network analyzer based on a modified six-port technique," in *Proc. IEEE Topical Conf. Wireless Sensors Sensor Netw. (WiSNet)*, Jan. 2015, pp. 23–25.

[60] K. Kim, N. Kim, S.-H. Hwang, Y.-K. Kim, and Y. Kwon, "A miniaturized broadband multi-state reflectometer integrated on a silicon MEMS probe for complex permittivity measurement of biological material," *IEEE Trans. Microw. Theory Techn.*, vol. 61, no. 5, pp. 2205–2214, May 2013.

[61] G. Vinci et al., "Six-port radar sensor for remote respiration rate and heartbeat vital-sign monitoring," *IEEE Trans. Microw. Theory Techn.*, vol. 61, no. 5, pp. 2093–2100, May 2013.

[62] K. Haddadi, M. M. Wang, C. Loyez, D. Glay, and T. Lasri, "Four-port communication receiver with digital IQ-regeneration," *IEEE Microw. Wireless Compon. Lett.*, vol. 20, no. 1, pp. 58–60, Jan. 2010.

[63] K. Haddadi, M. Wang, D. Glay, and T. Lasri, "Ultra wide-band four-port reflectometer using only two quadratic detectors," in *IEEE MTT-S Int. Microw. Symp. Dig.*, Jun. 2008, pp. 379–382.

[64] Analog Devices, Inc. (2017). *Wideband Synthesizer With Integrated VCO*. [Online]. Available: https://www.analog.com/media/en/technical-documentation/data-sheets/ADF4351.pdf

[65] Analog Devices, Inc. (2017). *1 MHz to 8 GHz, 70 dB Logarithmic Detector/Controller*. [Online]. Available: https://www.analog.com/media/en/technical-documentation/data-sheets/AD8318.pdf

Mayank Awasthi is currently pursuing the M.S. degree in ECE from the International Institute of Information Technology, Hyderabad, India.

He is currently working with the Center for VLSI and Embedded Systems Technology Lab, Hyderabad.

Syed Azeemuddin (Senior Member, IEEE) received the B.E. degree from MJ, Osmania University, Hyderabad, India, in 2003, and the M.S. and Ph.D. degrees from Southern Illinois University Carbondale, Carbondale, IL, USA, in 2005 and 2008, respectively.

He is currently an Associate Professor and the Head of CVEST, IIIT-Hyderabad, Hyderabad. His current research work include on-chip RF inductors, RF biosensors, high-energy systems, and RADAR detection.

Annesha Mazumder is currently pursuing the Ph.D. degree with the Center for VLSI and Embedded Systems, IIIT-Hyderabad, Hyderabad, India.

Mohammad Hashmi (Senior Member, IEEE) received the B.Tech. degree from Aligarh Muslim University, Aligarh, India, in 2001, the M.S. degree from the Darmstadt University of Technology, Darmstadt, Germany, in 2004, and the Ph.D. degree from Cardiff University, Cardiff, U.K, in 2009.

He had held research, engineering, and academic positions with the University of Calgary, Canada; Cardiff University; Thales Electronics GmbH, Germany; Philips Technology Center, Germany; and IIIT Delhi, India. He is currently an Associate Professor with Nazarbayev University, Kazakhstan. His research activities have led to one book, three U.S. patents (two pending), and over 260 journals and conference publications. His current research interests include the domain of advanced RF circuits for wireless applications (including wireless power transfer and energy harvesting), emerging RF circuits and applications, broadband linear and efficient power amplifiers for mobile and satellite applications, and high- and low-frequency instrumentation.

Dr. Hashmi is an Associate Editor of IEEE *Microwave Magazine*.